Nonlinear Raman vibrational excitation of a trapped ion

Heping Zeng,[1,2] Yuzhu Wang,[2] and Yusaburo Segawa[1]
[1]*Photodynamics Research Center (PDC), The Institute of Physical and Chemical Research (RIKEN), 19-1399 Koeji, Nagamachi, Aoba-ku, Sendai 980-0868, Japan*
[2]*Shanghai Institute of Optics and Fine Mechanics, P.O. Box 800-211, Shanghai, China*
(Received 9 September 1998)

Raman sideband excitations driven by counterpropagating Raman beams are analyzed for the trapped ion under the localization conditions in and beyond the Lamb-Dicke regime. Multiquantum vibrational couplings are demonstrated to produce significant effects on the Raman sideband transitions and the relevant Raman excitations of the trapped ion beyond the Lamb-Dicke regime. The quantum features of the vibrational states attained by exciting the motional ground state are closely associated with the nonlinear vibronic couplings, Raman excitation, and localization conditions. Quantum entanglement and quantum interference are discussed for the trapped ion under various Raman excitation and localization conditions. The results are compared with the recent experiments. Further experimental attempts are proposed to use the single trapped $^{25}Mg^{+}$ ion in a linear ion trap. [S1050-2947(99)07603-9]

PACS number(s): 32.80.Pj, 42.50.Vk, 42.50.Md, 32.80.Qk

I. INTRODUCTION

Recently, it has been of increasing interest to study the quantized motion of a single trapped ion for its intriguing applications in quantum optics [1–4]. In an ion trap, the center-of-mass motion of the ultracold single trapped ion can be approximately regarded as an ideal harmonic oscillator with discrete eigenstates. It is clear that the ionic internal excitation or deexcitation driven by classical laser fields is usually accompanied by vibronic couplings, which enables the realization of some cavity QED experiments with the quantized radiation fields being replaced by the quantized motion of the trapped ion [5]. Consider a two-level trapped ion interacting with a classical traveling- or standing-wave laser field tuned to the first motional sideband. The vibronic Jaynes-Cummings type [6,7] and nonlinear vibronic Jaynes-Cummings type couplings may be observed [8,9] in an ion trap in and beyond the Lamb-Dicke (LD) regime, respectively, where the LD regime is defined as a localization dimension much smaller than the wavelength of the relevant ionic transition.

Moreover, recent developments in laser cooling and trapping techniques, especially sideband laser cooling [10] and stimulated Raman sideband cooling techniques [11,12], have enabled experimental attainments of the motional ground state with high probabilities. Such a well-defined state may serve as the initial condition for preparing some interesting quantum motional states of trapped particles, such as Fock states [13–19], coherent states [18,20–22], vibrational ''Schrödinger cat'' states [23–25], and squeezed states [20–22,26]. In their remarkable experiments in the rf (Paul) ion trap [18,23], Wineland and his co-workers have proved the feasibility of implementing the first and second Raman sideband excitations to displace and squeeze the vibrational ground state, respectively. The Raman excitation schemes allow elimination of the electronic transitions from the dynamics of the system. It has already been demonstrated that the appropriately selected sequence of Raman sideband couplings closely correlated with the relevant internal spin states could produce entangled quantum-mechanical wave packets, and in particular vibrational ''Schrödinger cat'' states [23].

Consider a configuration where a single trapped ion interacts with two counterpropagating traveling-wave laser beams tuned far off any internal electronic resonances, with the corresponding wave-vector difference pointing to one of the principal trap axes of the ion trap, for example the z axis. Under sideband resonance, the laser beams will drive two-photon Raman transitions between vibrational levels. In the LD limit, if the two applied laser beams differ in frequency by ν (ν is the trap frequency along the z axis), the Raman excitation acts as a ''Raman motional displacement'' in the LD approximation, i.e., it displaces the initial vibrational ground state to a coherent motional state while the Raman excitation squeezes the initial vibrational ground state to a vacuum squeezed state of motion if the two applied laser beams differ in frequency by 2ν. However, the LD approximation becomes invalid for a trapped ion localized beyond the LD regime. In such a case the interference of the motional wave packets with the irradiating laser waves leads to nonlinear modification of the Raman sideband excitations. It was theoretically demonstrated that, when the spatial extension of the motional wave packet is comparable to the irradiating laser wavelength, there exists destructive interference between the motional wave packet and the laser wave. Such destructive interference may even cause the atom-field interaction to break down [27]. We note that the recent experiments [18,23] in connection with the preparation of coherent and vacuum squeezed motional states were performed in an ion trap slightly beyond the LD regime, with a typical LD parameter $\eta \approx 0.2$. The experimental results were simply analyzed using the LD approximation, taking no account of the nonlinear vibronic couplings. It seems to be important to provide more accurate theoretical analyses for the already-done experiments. Moreover, it is of experimental interest to check what kinds of motional states can be excited from a vibrational ground state by the nonlinearly modified Raman sideband interaction, what kinds of quantum feature the Raman excited motional states may exhibit, whether the non-

linearly modified Raman excitations can be used to study quantum entanglement and interference, whether the attained motional states can be used for further quantum optics experiments, and so on. This paper will address these questions. We will also discuss in detail the characteristics of the Raman sideband excitations for single trapped ions in and beyond the LD limit.

This paper is organized as follows. In Sec. II, a theoretical model is introduced. Section III discusses the quantum features of the nonlinearly excited vibrational states of the ionic motion. In Sec. IV, we discuss the quantum interference of the displaced motional states. A conclusion is given in Sec. V, where an experiment is proposed to use a single trapped $^{25}Mg^{+}$ ion in a miniature linear trap. In Appendix A, an approximate master equation is derived to describe the interaction of a trapped ion with two traveling-wave laser beams. Appendix B gives an efficient numerical procedure to integrate the Schrödinger equation in Sec. II.

II. THEORETICAL MODEL

We consider that a trapped ion interacts with two radiation fields of frequencies ω_{L1} and ω_{L2}. Assume that the propagating directions of the applied laser fields are arranged so that the wave-vector difference points along one of the principal trap directions, say, for example, the z axis. Hence vibronic Raman couplings only occur for the center-of-mass motion in the z dimension. Note that the three degrees of freedom of the center-of-mass motion in the three principal directions can be considered independently, and that the applied laser fields produce no observable effects on the center-of-mass motion in the x and y dimensions. We may therefore simply restrict ourselves to the one-dimensional motion in the z direction. If the laser frequencies are tuned far off any electronic resonances, the laser fields drive the off-resonant electronic transitions between an electronic ground state and intermediate states. As shown in Appendix A, a standard adiabatic elimination can be applied to intermediate states, and the interaction of the total system can be simplified as effective two-photon Raman couplings between vibrational levels. The Hamiltonian takes the form

$$H=H_{tp}+H_{\rm eff}, \tag{1a}$$

$$H_{tp}=\hbar\nu\left(a^{\dagger}a+\frac{1}{2}\right), \tag{1b}$$

$$H_{\rm eff}=\hbar R[e^{i(\Delta kz-\Delta\omega t)+i\phi}+\text{H.c.}], \tag{1c}$$

where H_{tp} and $H_{\rm eff}$ are the Hamiltonians for the ionic motion of the trapped ion and effective two-photon Raman couplings, respectively, $\Delta k=\mathbf{e}_z\cdot(\mathbf{k}_1-\mathbf{k}_2)$ and $\Delta\omega=\omega_{L1}-\omega_{L2}$ are the wave-vector difference along the z-direction ($\mathbf{e}_z$ denotes the unit vector in the z-direction) and frequency difference of the applied laser fields, respectively, $\mathbf{k}_1$ and $\mathbf{k}_2$ denote the laser wave vectors, R is the real (positive) effective two-photon coupling constant, ϕ is the phase difference of the two laser beams, and $a=[M\nu/(2\hbar)]^{(1/2)}[z+ip/(M\nu)]$ is the usual annihilation operator for the harmonic oscillator (z and p are position and momentum operators, respectively, and M is the ionic mass).

If the laser frequencies are tuned to the lth Raman sideband resonance, i.e., $\omega_{L1}-\omega_{L2}=l\nu$, the effective Hamiltonian of the Raman interaction can be simplified in the so-called rotating-wave approximation in the weak excitation regime, where the effective two-photon Rabi frequency R is much smaller than the trap frequency ν. In a rotating frame defined by the unitary transformation $H_{\rm eff}\rightarrow\mathcal{U}_0H_{\rm eff}\mathcal{U}_0^{\dagger}$ with $\mathcal{U}_0=\exp(-i\nu ta^{\dagger}a)$, the effective Hamiltonian takes the form [27,28]

$$\mathcal{H}_{l,\phi}=\hbar Re^{i\phi-\eta^2/2}\sum_{m=0}^{+\infty}\frac{(i\eta)^{2m+l}}{m!(m+l)!}(a^{\dagger})^m a^{m+l}+\text{H.c.}, \tag{2}$$

where $\eta=[\hbar(\Delta k)^2/2M\nu]^{1/2}$ is the LD parameter for the two-photon transitions. We have expanded the factor $\exp(i\Delta kz)=\exp[i\eta(a^{\dagger}+a)]$ in orders of η [27,28]

$$e^{i\Delta kz}=\exp\left(-\frac{\eta^2}{2}\right)\sum_{l\geqslant 0}^{+\infty}\sum_{m=0}^{+\infty}\frac{(i\eta)^{2m+l}}{m!(l+m)!}\times[(a^{\dagger})^m a^{m+l}+(a^{\dagger})^{m+l}a^m]. \tag{3}$$

Terms containing time-dependent factors such as $\exp(i\kappa\nu t)$ are neglected in the spirit of the vibrational rotating-wave approximation, where κ is a nonzero integer. It should be reminded that sideband transitions $|n+l\rangle\rightarrow|n\rangle$ with $|l|\geqslant 2$ are approximately forbidden for a trapped ion in the LD regime. But for the case of large LD parameters, the LD approximation does not hold. The multiquantum motional excitation causes nonlinearity in sideband couplings [27,28]. For example, for the first sideband transitions ($|n\rangle\rightarrow|n+1\rangle$), there exist a lot of terms of excitation described by $(a^{\dagger})^{m+1}a^m$, each proportional to $\eta^{2m+1}(m=0,1,2,\ldots)$. Such vibrational multiquantum couplings contribute significantly to Raman sideband transitions. The associated vibronic coupling constant between $|n\rangle$ and $|n+l\rangle$ is actually proportional to

$$\Omega_{n,n+l}=\langle n|\exp[i\Delta kz]|n+l\rangle=\exp\left[-\frac{\eta^2}{2}\right](i\eta)^l\sqrt{\frac{n!}{(n+l)!}}L_n^l(\eta^2)\quad(\text{for } l\geqslant 0), \tag{4}$$

where L_n^l is an associated Laguerre polynomial [27,28].

The time evolution of the quantized motion is governed by the time evolution operator

$$\mathcal{U}_{l,\phi}(t)\equiv\exp\left(\frac{1}{i\hbar}\mathcal{H}_{l,\phi}t\right). \tag{5}$$

From the initial vibrational ground state $|0\rangle$, the trapped ion is excited to $|\psi_l(t)\rangle_{\phi}\equiv\mathcal{U}_{l,\phi}(t)|0\rangle$ after a Raman interaction with a duration t. Numerically, $|\psi_l(t)\rangle_{\phi}$ can be calculated by solving the Schrödinger equation $i\hbar\partial|\psi_l(t)\rangle_{\phi}/\partial t=\mathcal{H}_{l,\phi}|\psi_l(t)\rangle_{\phi}$ with the initial condition $|\psi_l(t=0)\rangle_{\phi}=|0\rangle$. An efficient numeric procedure is presented in Appendix B for solving this equation.

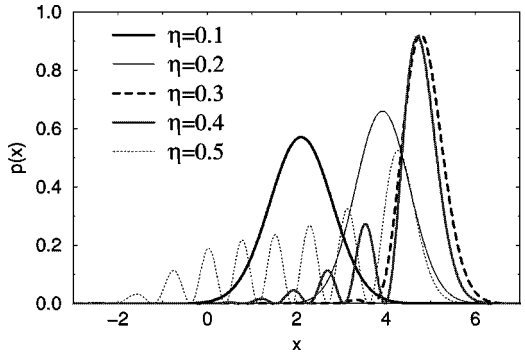

FIG. 1. The spatial probability distribution $p(x)=|\langle x|\psi_1(t)\rangle_{\phi=0}|^2$ of a vibrational wave packet excited by Raman beams with $\phi=0.0$ and $Rt=15.0$, where x is defined as $x=z/a_0$ with $a_0=\sqrt{\hbar/(M\nu)}$. The ion is trapped with the LD parameters $\eta=0.1$, 0.2, 0.3, 0.4, and 0.5, respectively.

III. RESULTS AND DISCUSSIONS

In what follows, we will demonstrate that the nonlinearly modified Raman vibrational excitations can be used to create some novel nonclassical motional states of a trapped ion from the initial vibrational ground state.

A. The first sideband Raman displacement

For a trapped ion under localization condition in the LD limit, a displacement operator can be experimentally realized by the use of displacement Raman beams of traveling-wave radiation fields which differ in frequency by ν [23]. The applied laser fields create Raman couplings between vibrational levels, which are governed by a rotating-wave-approximation Hamiltonian as $\mathcal{H}_{1,\phi}\approx i\hbar R\eta a e^{i\phi}-i\hbar R\eta a^{\dagger}e^{-i\phi}$ to the first order of η. Such Raman interaction will excite the initial vibrational ground state to the state $|\psi(t)\rangle=\mathcal{U}_{1,\phi}(t)|0\rangle$, where the time-evolution operator $\mathcal{U}_{1,\phi}(t)$ approximates the displacement operator $\mathcal{U}_{1,\phi}(t)\approx D(-Rt\eta e^{-i\phi})$, with the displacement operator being defined by $D(\alpha)=\exp(\alpha a^{\dagger}+\alpha^{*}a)$. $|\psi(t)\rangle$ is therefore a coherent state with an average vibrational number $\langle n(t)\rangle=|Rt\eta|^2$ and phase $e^{-i\phi+i\pi}$. Note that all the above analyses are based upon the LD perturbation approximation to the first order of the LD parameter η. Moreover, the polarization of the applied laser beams and the internal ground-state sublevel can be properly chosen so that the displacement beams only affect the motional states correlated with the selected ground-state sublevel [23]. The attained coherent motional state is then correlated with the relevant electronic ground state.

Beyond the LD regime, the vibronic couplings include contribution from many multiquantum processes such as $(a^{\dagger})^m a^{m+l}$ and $(a^{\dagger})^{m+l}a^m$. The time-evolution operator $\mathcal{U}_{1,\phi}(t)$ is obviously different from the displacement operator, and $|\psi_1(t)\rangle_{\phi}=\mathcal{U}_{1,\phi}(t)|0\rangle$ is no longer a coherent state of motion. Note that $\mathcal{U}_{1,\phi}(t)$ can be simplified as a displacement operator when only terms of the first order of η are considered. In this sense, $\mathcal{U}_{1,\phi}(t)$ may be regarded as an extended displacement operator. Because the vibrational mode is nonlinearly coupled during the Raman excitations, we may term $\mathcal{U}_{1,\phi}$ as a ''nonlinear displacement operator.''

Figure 1 gives the spatial probability distributions of the wave packets $|\psi_1(t)\rangle_{\phi=0}$ under various localization conditions ($\eta=0.1$–0.5), and with the Raman interaction areas $Rt=15.0$ [23]. For small LD parameters, the wave packet $|\psi_1(t)\rangle_{\phi}$ is approximately of Gaussian shape, and the corresponding wave-packet state approximates a coherent one. Note that $\eta=0.2$ and $Rt=15.0$ corresponds to the experimental situation in Ref. [23]. For large LD parameters, the wave packets become spatially spread. Each wave packet may even consist of many separate subpackets [30].

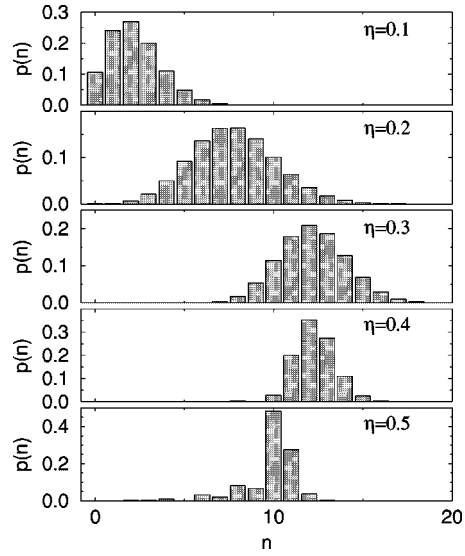

FIG. 2. The occupation distribution of vibrational states $\mathcal{U}_{1,\phi=0}(t)|0\rangle$, with Raman excitation area $Rt=15.0$, driven by two Raman displacement beams which differ in frequency by the trap frequency along the associated principal trap axis (ν). The LD parameters are selected as $\eta=0.1$, 0.2, 0.3, 0.4, and 0.5, respectively.

On the basis of vibrational Fock states, $|\psi_1(t)\rangle_{\phi}$ can be expanded as a coherent superposition $|\psi_1(t)\rangle_{\phi}=\Sigma_{n=0}c_n(t)|n\rangle$ with $c_n(t)=\langle n|\psi_1(t)\rangle_{\phi}$. The coefficients $c_n(t)$ depends on the details of the Raman interaction. The occupation probability in the vibrational state $|n\rangle$ is given by $p(n)=|c_n(t)|^2$. Figure 2 gives an example of the occupation distribution of the displaced motional states $|\psi_1(t)\rangle_{\phi=0}$ with Raman pulse $Rt=15.0$, where the LD parameters are selected as $\eta=0.1$, 0.2, 0.3, 0.4, and 0.5, respectively. Note that $p(n)=\exp(-|\alpha|^2)|\alpha|^{2n}/n!$ for a coherent motional state $|\alpha\rangle$. It is clear that, for the case of a large LD parameter, the occupation distribution of $|\psi_1(t)\rangle_{\phi=0}$ deviates from that of any coherent motional states.

The quantum statistics of $|\psi_1(t)\rangle_{\phi}$ can be characterized by $Q=(\langle\hat{N}^2\rangle-\langle\hat{N}\rangle^2)/\langle\hat{N}\rangle-1$, which satisfies $Q=0$ for the Poissonian distribution, $Q>0$ for the super-Poissonian distribution, and $Q<0$ for the sub-Poissonian distribution, where $\hat{N}=a^{\dagger}a$. In Fig. 3, Q is plotted as a function of Raman excitation area Rt, which clearly shows that the attained vibrational wave packet may be of sub- or super-Poissonian statistics dependent on the details of the Raman excitation. It is interesting to note that Q is negative ($Q\approx-0.27$) for the displaced motional state attained in Ref. [23] with $\eta\approx0.2$ and $Rt\approx15.0$. The quantum fluctuations of the dimensionless momentum $\tilde{p}=i(a^{\dagger}-a)/2$ and position $\tilde{z}=(a+a^{\dagger})/2$ are shown in Figs. 4(a) and 4(b), respectively, where motional

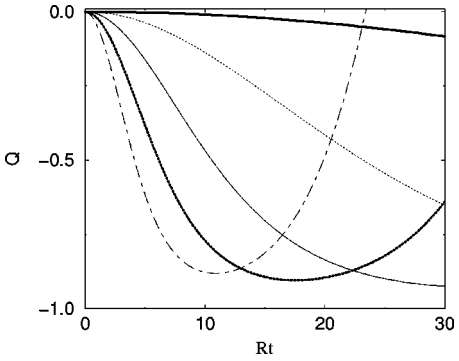

FIG. 3. The vibrational Q function of the state $\mathcal{U}_{1,\phi=0}(t)|0\rangle$ of the trapped ion with the LD parameters $\eta=0.1$ (wide solid line), $\eta=0.2$ (thin dotted line), $\eta=0.3$ (thin solid line), $\eta=0.4$ (wide dotted line), and $\eta=0.5$ (dotted-dashed line), respectively, for different Raman pulses ($Rt=0.0\sim30.0$).

squeezing is demonstrated to occur in the position direction with appropriate Raman displacements. Note that $|\psi_1(t)\rangle_\phi$ is no longer a minimum-uncertainty vibrational state, i.e., $\langle(\Delta\tilde{z})^2\rangle\langle(\Delta\tilde{p})^2\rangle>1/16$. Particularly, the displaced motional state with $\eta\approx0.2$ and $Rt\approx15.0$ is a position-squeezed one. This can also be seen from Fig. 1, which indicates such a wave-packet state actually has a narrower shape than that of a coherent one [13–17].

B. The second sideband Raman excitations

Let us examine the nonlinearly modified second-sideband Raman excitations of the vibrational ground state. Figure 5 depicts the spatial probability distributions of the motional wave packets $|\psi_2(t)\rangle_{\phi=\pi/2}$ under various localization and Raman excitation conditions. For a small LD parameter, $|\langle z|\psi_2(t)\rangle_{\phi=\pi/2}|^2$ is of a Gaussian shape. Note that a ''vacuum squeezed'' state $|\psi_{\rm sq}\rangle=\exp[r/2(a^{\dagger2}-a^2)]|0\rangle$ can be expressed in the position representation as $\langle z|\psi_{\rm sq}\rangle$

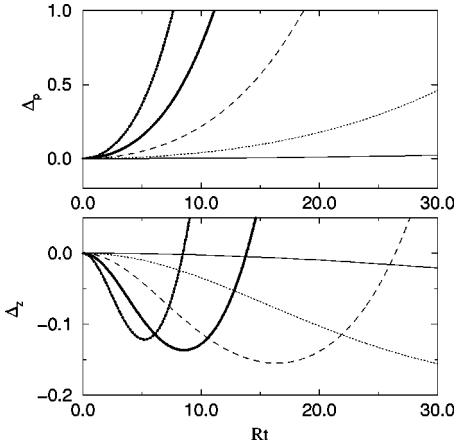

FIG. 4. The quantum fluctuations $\Delta_z=\langle(\Delta\tilde{z})^2\rangle-1/4$ and $\Delta_p=\langle(\Delta\tilde{p})^2\rangle-1/4$ of the dimensionless position and momentum operators $\tilde{z}=(a+a^\dagger)/2$ and $\tilde{p}=(a-a^\dagger)/2i$ for a vibrational state excited by different Raman pulses ($Rt=0.0\sim30.0$ and $\phi=0.0$), respectively. The LD parameters of the trapped ion are chosen as $\eta=0.1$ (thin solid line), $\eta=0.2$ (thin dotted line), $\eta=0.3$ (thin dashed line), $\eta=0.4$ (wide solid line), and $\eta=0.5$ (wide dotted line), respectively.

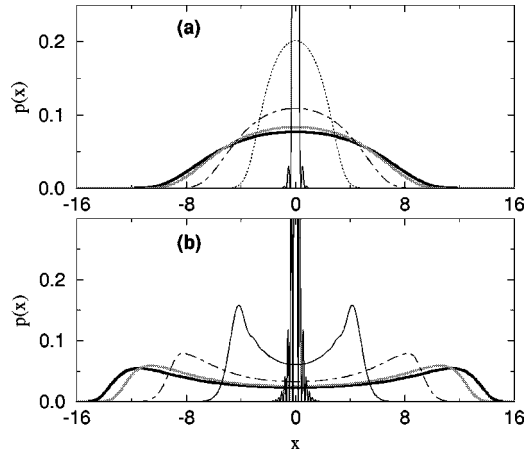

FIG. 5. The spatial probability distributions of $|\psi_2(t)\rangle_{\phi=\pi/2}$ and the associated free evolutions for $\eta=0.2$ and $Rt=50.0$ (a) and $Rt=80.0$ (b), respectively. $p(x)$ is given by $p(x)=|\langle x|\psi_2(t)\rangle_{\phi=\pi/2}|^2$, where x is defined as $x=z/a_0$ with $a_0=\sqrt{\hbar/(M\nu)}$. The free time evolution after the preparation ($t_f=0$) is shown in the spatial probability distributions for some selected time points $t_f=0.0$ (solid line), $T/8$ (dotted line), $T/4$ (dot-dashed line), $3T/8$ (gray line), and $T/2$ (thin solid line) ($T=\pi/\nu$), respectively.

$=\psi(z,\sigma)=[1/(\pi\sigma^2)^{1/4}]\exp(-z^2/\sigma^2)$ with $\sigma=\exp(-r)$. For example, for a LD parameter $\eta=0.2$ and Raman pulse area $Rt=50.0$, we can get a squeezed wave packet as shown in Fig. 5(a). In a recent experiment [18], a nearly ''vacuum squeezed'' state has been attained with second-sideband Raman excitations. On the other hand, a double-peaked spatial distribution can be attained with some larger Raman pulse areas. Figure 5(b) gives the spatial probability distribution for $Rt=80.0$. Clearly, a double-peaked wave packet differs from a Gaussian-shaped ''vacuum squeezed'' one.

For larger LD parameters, the nonlinearly modified second-sideband Raman excitations with appropriate areas Rt can even split the motional ground state into two spatially separate wave packets. In Fig. 6, we plot the spatial probability distributions of the wave packets for LD parameters and Raman pulse areas $\eta=0.3$ and $Rt=50.0$ (a), $\eta=0.4$ and $Rt=25.0$ (b), and $\eta=0.5$ and $Rt=15.0$ (c), respectively. The free time evolution of the two spatially separate wave packets is also shown at some time points ($t_f=0$, $T/8$, $T/4$, $3T/8$, and $T/2$ with $T=\pi/\nu$) after the Raman interaction, where $t_f=0$ represents the time point just after the Raman interaction is switched off.

Numerical calculations show that there exists a particular range of Rt with which the second-sideband Raman excitations are approximately equivalent to a coherent splitter of the motional ground (Gaussian-shaped) wave packet. For example, Fig. 7 indicates that spatial splittings can be attained with $Rt=15.0$–30.0 and $\eta=0.4$ [29].

Physically, the splitting originates in the quantum interference between vibrational levels. If the motional state is prepared in a proper superposition of vibrational Fock states, there may exist destructive interferences in a wide range around the center point of the trap, leading to a vanishing local spatial probability. Therefore the resulting wave packet consists of two spatially separate parts. The free time evolution of the motional states changes the relative phases

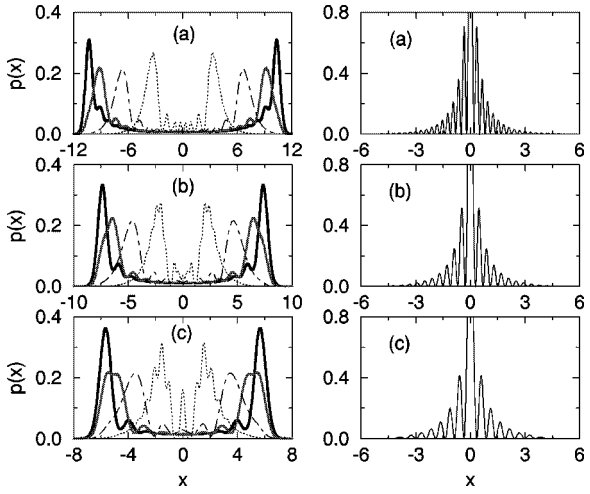

FIG. 6. The spatial probability distributions of $|\psi_2(t)\rangle_{\phi=\pi/2}$ and the associated free time evolution for $\eta=0.3$ and $Rt=50.0$ (a), $\eta=0.4$ and $Rt=25.0$ (b), and $\eta=0.5$ and $Rt=15.0$ (c), respectively. For clarity, (a), (b), and (c) are all split into two graphs, respectively. $p(x)$ is given by $p(x)=|\langle x|\psi_2(t)\rangle_{\phi=\pi/2}|^2$, where x is defined as $x=z/a_0$ with $a_0=\sqrt{\hbar/(M\nu)}$. The free time evolution after the preparation ($t_f=0$) is shown in the spatial probability distributions for some selected time points $t_f=0.0$ (solid line), $T/8$ (gray line), $T/4$ (dot-dashed line), $3T/8$ (dotted line), and $T/2$ (thin solid line) ($T=\pi/\nu$), respectively.

of the vibrational Fock-state components, and thus changes the interference features. When the two parts spatially overlap at the center of the trap during the oscillation, interference fringes can be expected in the spatial probability distribution. As a whole, by the use of the nonlinearly modified second-sideband Raman excitations, the motional ground state (Gaussian-shaped wave packet) is coherently split into two symmetric vibrational wave packets localized at distinguishable positions. Each of the split packets undergoes the same motion but with a phase difference of π. The two

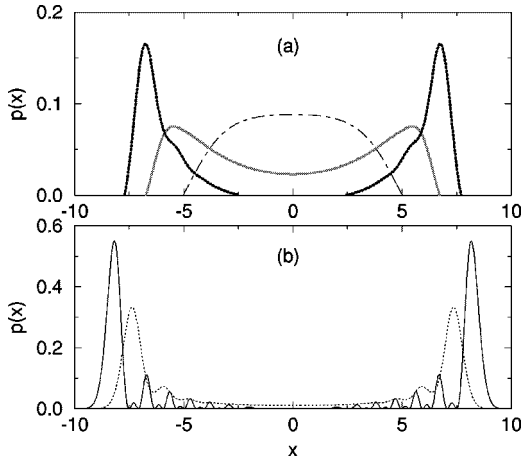

FIG. 7. The spatial probability distributions of $|\psi_2(t)\rangle_{\phi=\pi/2}$ at $t_f=0$ for $\eta=0.4$. The Raman pulse area is selected as $Rt=10.0$ (dot-dashed line), 15.0 (gray line), 20.0 (wide dotted line), 25.0 (dotted line), and 30.0 (solid line), respectively. For clarity, the graph is split into two parts, (a) and (b). $p(x)$ is given by $p(x)=|\langle x|\psi_2(t)\rangle_{\phi=\pi/2}|^2$, where x is defined as $x=z/a_0$ with $a_0=\sqrt{\hbar/(M\nu)}$.

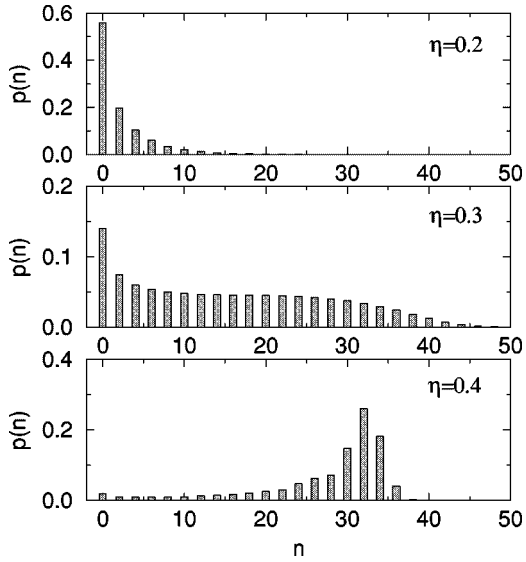

FIG. 8. The occupation probability $p(n)$ of the vibrational state $\mathcal{U}_{2,\phi}(t)|0\rangle$ with $\phi=\pi/2$ and $Rt=30.0$. The LD parameters for the trapped ion are $\eta=0.2$, 0.3, and 0.4, respectively. $p(n)=|\langle n|\psi_2(t)\rangle_{\phi=\pi/2}|^2$.

resulting packets pass through and thus interfere with each other near the center point of the harmonic trap. Quantum interferences induce interference fringes in the spatial probability distribution, which are determined by the phase difference between the de Broglie waves associated with the two split wave packets. Based on this motional wave-packet splitting, one may build an ion-trap interferometer to observe the quantum interference between the de Broglie waves associated with the two motional wave packets [30].

Let us now discuss the quantum features of the second-sideband excitation on the basis of the vibrational Fock states. For a small LD parameter, the related effective Hamiltonian approximates $\mathcal{H}_{2,\phi}=-\hbar R\exp(i\phi)\eta^2a^2/2+\text{H.c.}$ up to the second order of η, and therefore $|\psi_2(t)\rangle_\phi$ is approximately a ''vacuum squeezed state,'' i.e., $|\psi_2(t)\rangle_\phi=S(\epsilon)|0\rangle$, where $S(\epsilon)=\exp[(\epsilon a^{\dagger2}-\epsilon^* a^2)/2]$ is the ''squeeze'' operator, with $\epsilon\equiv r\exp(i\theta)=i\eta^2Rt\exp(-i\phi)$ ($r=\eta^2Rt$ is the squeezing parameter and $\theta=\pi/2-\phi$ is the squeezing angle). For example, the squeezed motional states attained in the recent experiment [18] (for a LD parameter $\eta\approx0.2$) were fitted to have the vibrational occupational distribution $p_{2n}=\text{sech}\,r(2n)!(\tanh r)^{2n}/(2^n n!)^2$, with $\beta\equiv\exp(2r)=40\pm10$ (i.e., $Rt=45\pm3$). However, for a large LD parameter, the Raman interaction produces a complicated superposition of vibrational states (see Fig. 8). The occupation distribution for such a superposed motional state is shown in Fig. 8 with the LD parameters $\eta=0.2$, 0.3, and 0.4, respectively. The population distribution is restricted to the even vibrational states. One may see that the Raman excitation of the trapped ion with a relatively large LD parameter gives rise to a population distribution obviously deviating from that of an ideal vacuum squeezed vibrational state. The difference originates in the nonlinear modification of the associated second-sideband vibronic coupling constants between vibrational levels $|n\rangle$ and $|n+2\rangle$, which are proportional to $|\Omega_{n,n+2}|=|\langle n|\exp[i\eta(a+a^\dagger)]|n+2\rangle|=\frac{1}{2}\eta^2\sqrt{(n+1)(n+2)}+O(\eta^4)$. When n is large and η is

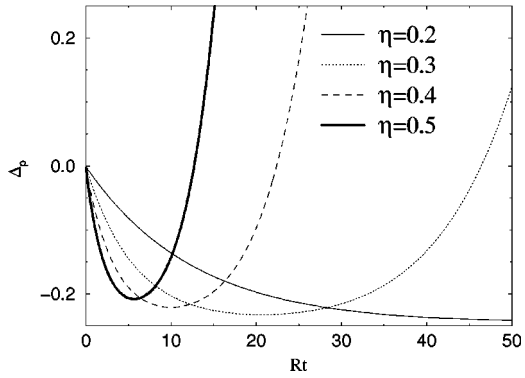

FIG. 9. The quantum fluctuation $\Delta_p=\langle(\Delta\tilde{p})^2\rangle-1/4$ of the dimensionless momentum operator $\tilde{p}=(a-a^\dagger)/2i$ of the vibrational state $\mathcal{U}_{2,\phi=\pi/2}(t)|0\rangle$ of a trapped ion with the LD parameters $\eta=0.2$, 0.3, 0.4, and 0.5, respectively. The motional state is excited by Raman pulses tuned to the second sideband resonance ($Rt=0.0$–50.0).

not too small, the nonlinear terms included in $O(\eta^4)$ produce significant effects on the Raman excitation.

The intriguing quantum statistics are illustrated in Fig. 9. With some particular Raman excitations, quadrature vibrational squeezing for the dimensionless momentum operator $\tilde{p}=i(a^\dagger-a)/2$ can be produced. Only in the first order of the LD expansion do the quantum fluctuations of the dimensionless position and momentum operators ($\tilde{z}$ and $\tilde{p}$) of the state $\mathcal{U}_{2,\phi}(t)|0\rangle$ approximately satisfy the minimum-uncertainty relation $\langle(\Delta\tilde{z})^2\rangle\langle(\Delta\tilde{p})^2\rangle=1/16$, which is a signature of the vacuum squeezed state. The state $\mathcal{U}_{2,\phi}(t)|0\rangle$ can then be thought of as an extension of the ''vacuum squeezed state'' of motion of the trapped ion beyond the LD regime.

C. *l*th ($l>2$) sideband Raman excitations

In a similar way, by the use of Raman beams which differ in frequency by $l\nu$, the initial ground state of motion is driven to $|\psi_l(t)\rangle_\phi=\mathcal{U}_{l,\phi}(t)|0\rangle$ after a Raman interaction with a duration t.

In Fig. 10, we plot the vibrational occupation probability

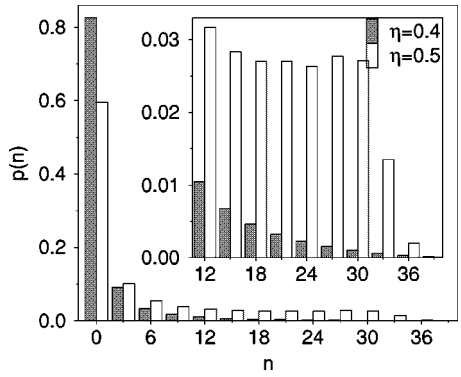

FIG. 10. The occupation distribution of a vibrational wave packet $\mathcal{U}_{3,\phi=0}(t)|0\rangle$ of a trapped ion with the LD parameters $\eta=0.4$ and 0.5, respectively, which is excited by Raman pulses ($Rt=20.0$) with a frequency difference of 3ν. The inset is the replot of the occupation distribution for vibrational levels $n\geqslant 12$ in a small $p(n)$ scale.

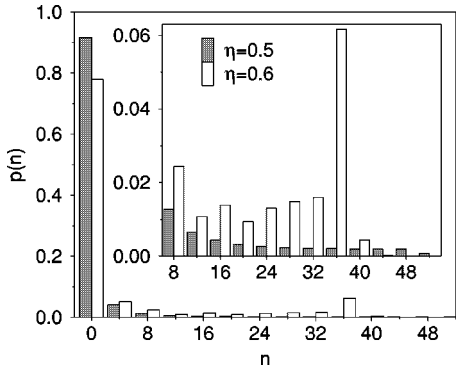

FIG. 11. The occupation distribution of the vibrational state $\mathcal{U}_{4,\phi=0}(t)|0\rangle$ of a trapped ion with the LD parameters $\eta=0.5$ and 0.6, respectively, driven by Raman beams which differ in frequency by 4ν and have excitation area $Rt=20.0$. The inset is the replot of the occupation distribution for vibrational levels $n\geqslant 8$ on a small $p(n)$ scale.

for the motional state $|\psi_3(t)\rangle_\phi$ of the trapped ion with the LD parameters $\eta=0.4$ and 0.5, respectively. Figure 11 illustrates the occupation distribution of the vibrational state $|\psi_4(t)\rangle_\phi$ with the LD parameters $\eta=0.5$ and 0.6, respectively. From the occupation distributions of the states $|\psi_3(t)\rangle_\phi$ and $|\psi_4(t)\rangle_\phi$, one can see that the main portion of the population is still in the vibrational ground state for both cases. A small portion of the population distributes among the Fock states $|n=3\kappa\rangle$ for $|\psi_3(t)\rangle_\phi$ and $|n=4\kappa\rangle$ for $|\psi_4(t)\rangle_\phi(\kappa=1,2,\ldots,)$, respectively. The weak vibrational excitation can be easily understood by considering $\mathcal{H}_{l,\phi}\propto\eta^l/(l!)+O(\eta^{l+1})$.

Both $|\psi_3(t)\rangle_\phi$ and $|\psi_4(t)\rangle_\phi$ possess no quadrature squeezing. One can readily get the quantum fluctuations of the operators $\tilde{z}$ and $\tilde{p}$, $\langle(\Delta\tilde{z})^2\rangle\equiv\langle\tilde{z}^2\rangle-\langle\tilde{z}\rangle^2=1/4$, and $\langle(\Delta\tilde{p})^2\rangle\equiv\langle\tilde{p}^2\rangle-\langle\tilde{p}\rangle^2=1/4$, for $|\psi_3(t)\rangle_\phi$ and $|\psi_4(t)\rangle_\phi$, respectively. Therefore both $|\psi_3(t)\rangle_\phi$ and $|\psi_4(t)\rangle_\phi$ are minimum-uncertainty motional wave packets. It is interesting to check their higher-order squeezing characteristics. Let us define the amplitude-squared operators

$$y_1=[(a^\dagger)^2\exp(-i2i\nu t)+a^2\exp(2i\nu t)]/2$$

and

$$y_2=i[(a^\dagger)^2\exp(-i2i\nu t)-a^2\exp(2i\nu t)]/2.$$

Clearly, y_1 and y_2 fulfill the commutation relation $[y_1,y_2]=i(2\hat{N}+1)$ and the uncertainty relation $\langle\Delta y_1\rangle\langle\Delta y_2\rangle\geqslant\langle\hat{N}+1/2\rangle$ [31]. Note that for the states $|\psi_3(t)\rangle_\phi$, the quantum fluctuations satisfy $\langle(\Delta y_1)^2\rangle=\langle(\Delta y_2)^2\rangle=\langle\hat{N}+1/2\rangle$, i.e., there is no squeezing for the amplitude-squared operators. Figure 12 shows the quantum fluctuation of the amplitude-squared operator (y_1) of the motional state $|\psi_4(t)\rangle_\phi$ under various Raman excitation conditions, which indicates the existence of amplitude-squared squeezing, i.e., $\langle(\Delta y_1)^2\rangle<\langle\hat{N}+1/2\rangle$, in some Raman sideband excitation regimes. Such states may be useful to study the effects caused by the amplitude-squared squeezing.

To the lowest order of η, the effective Hamiltonian $\mathcal{H}_{l,\phi}$ takes the form $\mathcal{H}_{l,\phi}\approx\hbar Re^{i\phi}(i\eta)^l a^l/l!+\text{H.c.}$, for example,

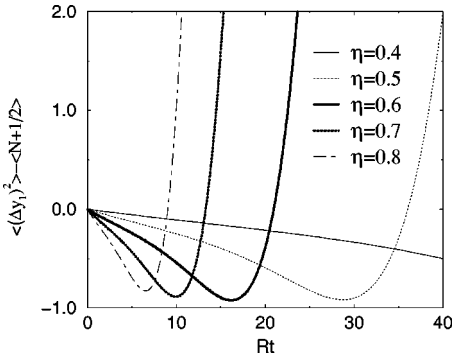

FIG. 12. The quantum fluctuation $\langle(\Delta y_1)^2\rangle-\langle\hat{N}+1/2\rangle$ ($\hat{N}=a^{\dagger}a$ represents the vibrational phonon number operator) of the dimensionless amplitude-squared operator $y_1=[(a^{\dagger})^2e^{-i2\nu t}+a^2e^{i2\nu t}]/2$ of the vibrational state $\mathcal{U}_{4,\phi=0}(t)|0\rangle$ driven by Raman pulses $Rt=20.0$. The LD parameters of the trapped ion are selected as $\eta=0.4$, 0.5, 0.6, 0.7, and 0.8, respectively.

for the case of $l=4,\mathcal{H}_{4,\phi}\approx\hbar R\,\eta^4e^{i\phi}a^4/24+$H.c. With small LD parameters, $\mathcal{H}_{l,\phi}\propto\eta^l$ has small vibrational coupling strengths. For those Raman sideband excitations to be experimentally observable, relatively large LD parameters should be used. We will discuss the experimental feasibility later on.

IV. ENTANGLED STATES OF MOTION

Following the procedures used in Ref. [23], one may prepare some interesting entangled states of motion. As a practical example, we consider Raman interactions in a single trapped $^{25}Mg^{+}$ ion. Assume that the trapped ion is prepared initially in the motional ground state and in an equal superposition of the internal electronic states, i.e., $(|g_1\rangle+e^{i\mu}|g_2\rangle)/\sqrt{2}$, with $|g_1\rangle$ and $|g_2\rangle$ being the internal ground-state sublevels such as $^2S_{1/2}|F=2,m_F=2\rangle$ and $|F=3,m_F=3\rangle$, respectively. If counterpropagating σ^+-polarized displacement beams are used to couple the internal transitions from $^2S_{1/2}|F=2,m_F=2\rangle$ to the virtual (off-resonant) state $^2P_{1/2}|F=3,m_F=3\rangle$, the Raman interaction excites only the motional states of the trapped ion in the internal ground state $|g_1\rangle$. At first, such counterpropagating σ^+-polarized displacement beams (with phase difference ϕ) are used to excite the motion correlated with $|g_1\rangle$ to a motional state $|\psi_1\rangle_{\phi}$. And then copropagating beams are applied to produce π-pulse Raman pumping between $|g_1\rangle$ and $|g_2\rangle$ to exchange population of the internal states in the superposition. After the population exchange, the internal states $|g_1\rangle$ and $|g_2\rangle$ become correlated with the motional states $|0\rangle$ and $|\psi_1\rangle_{\phi}$, respectively. The displacement beams (with phase difference ϕ') are then switched on to excite the motion correlated with the $|g_1\rangle$ component to a second motional state $|\psi_1\rangle_{\phi'}$. After that, the total system is in a superposition of two independent motional states, each correlated with an internal state of the ion, i.e., the total system is in the entangled state

$$|\Psi_1\rangle=\frac{|g_2\rangle\otimes|\psi_1\rangle_{\phi}+e^{i\mu'}|g_1\rangle\otimes|\psi_1\rangle_{\phi'}}{\sqrt{2}},\qquad(6)$$

with μ' depending on μ and the Raman couplings. The correlation in such an entangled state is not only interesting in quantum measurements, but also in reduction of quantum noise in spectroscopy [26]. For relatively small values of the LD parameter or for a small Raman excitation area when the attained motional states $|\psi_1\rangle_{\phi}$ and $|\psi_1\rangle_{\phi'}$ still possess macroscopic features, the entangled state corresponds to a mesoscopic superposition of quantum or even nonclassical motional wave packets macroscopically localized in spatially separated positions, which may be useful to study the quantum decoherence [32,33].

The two motional states can be combined with the use of a Raman $\pi/2$-pulse pumping between $|g_1\rangle$ and $|g_2\rangle$ to yield $|\Psi\rangle=|g_2\rangle|S_-\rangle-i|g_1\rangle|S_+\rangle$ [23], with

$$|S_{\pm}\rangle\equiv\frac{|\psi_1\rangle_{\phi}\pm e^{i\delta}|\psi_1\rangle_{\phi'}}{2},\qquad(7)$$

where δ depends on μ' and the relative phases of Raman pumping beams. This entangled state is generally not a ''Schrödinger cat'' state [23] as in Schrödinger's original thought experiment [34], since $|\psi_1\rangle_{\phi}$ and $|\psi_1\rangle_{\phi'}$ are no longer coherent states of motion for a trapped ion localized beyond the LD regime. For small LD parameters, it is still possible for $|\psi_1\rangle_{\phi}$ and $|\psi_1\rangle_{\phi'}$ to be spatially confined at separate positions. On the other hand, for large LD parameters, as already indicated in Fig. 1, both $|\psi_1\rangle_{\phi}$ and $|\psi_1\rangle_{\phi'}$ may be spatially spread so widely that spatial overlapping may occur for some portions of the wave packets.

Some interesting questions are worth addressing with regard to the motional superposition. One is whether the mesoscopic superposition gives rise to observable quantum interferences, even when $|\psi_1\rangle_{\phi}$ and $|\psi_1\rangle_{\phi'}$ are not coherent states of motion, for example, even when the wave packets are spatially wide-spread or squeezed ones. Another question is whether the spatial overlapping of some portions (particularly some subpackets) of the widespread wave packets can also cause the occurrence of quantum interferences.

In Fig. 13, we plot the spatial probability distribution of the superposition state $[|\psi_1(t)\rangle_{\phi=0}+|\psi_1(t)\rangle_{\phi=\pi}]/2$ and its free time evolution after the preparation. As a typical case for relatively small LD parameters, we consider the case of $\eta\approx0.2$ and $Rt\approx15.0$ [23] in Fig. 13(a). It is clear that the two symmetric vibrational wave packets $|\psi_1(t)\rangle_{\phi=0}$ and $|\psi_1(t)\rangle_{\phi=\pi}$ are initially localized at separate positions, and that both oscillate in the trap after the preparation. The associated oscillations differ in phase by π. The motion of the wave packet results obviously from the confinement of the trap potential. The two packets pass through each other near the center point of the harmonic trap. Since there exists coherence between the two packets, quantum interferences occur instead of a simple spatial overlapping when the two motional wave packets come close together. The quantum interferences induce interference fringes in the spatial probability distribution. As in the standard interferometer or atomic interferometer [35], the interference fringes are determined by the phase difference between the de Broglie waves associated with the two separate wave packets. Figure 13(b) gives an example for the cases of large LD parameters, where $\eta=0.4$ and $Rt=15.0$ are chosen. One can see that the widespread wave packets can still interfere with each other,

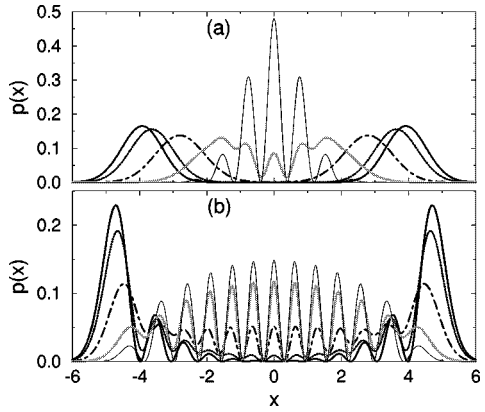

FIG. 13. The free time evolution of the superposition state $[|\psi_1(t)\rangle_{\phi=0}+|\psi_1(t)\rangle_{\phi=\pi}]/2$ after the preparation ($t_f=0$) for (a) $\eta=0.2$ and (b) $\eta=0.4$, respectively. Both $|\psi_1(t)\rangle_{\phi=0}$ and $|\psi_1(t)\rangle_{\phi=\pi}$ are prepared by displacing the motional ground state with Raman excitation areas $Rt=15.0$. The free time evolution is shown in the spatial probability distributions of the superposition state for some selected time points, $t_f=0.0$ (solid line), $T/8$ (dotted line), $T/4$ (dot-dashed line), $3T/8$ (gray line), and $T/2$ (thin solid line) ($T=\pi/\nu$), respectively. x is defined by $x=z/a_0$ with $a_0=\sqrt{\hbar/(M\nu)}$.

and the spatial overlapping of some subpackets can also result in interference fringes in the spatial distribution. It should be pointed out that there may be no distinct stages to separate splitting and interfering periods of the wave packets, when the Raman displacements become so complicated (for example, for very large LD parameters or long Raman interaction duration) that the displaced wave packets $|\psi_1(t)\rangle_{\phi=0}$ and $|\psi_1(t)\rangle_{\phi=\pi}$ initially interfere and become spatially indistinguishable [30].

As has been already demonstrated in Ref. [23], the quantum interferences can be directly measured by detecting the probability $P(\phi,\phi')\equiv\langle S_-|S_-\rangle$. Figure 14 gives the calculated signal

$$P(\varphi)\equiv P(\phi=-\varphi/2,\phi'=\varphi/2)$$
$$=(\langle\psi_1|_{-\varphi/2}-\langle\psi_1|_{\varphi/2})(|\psi_1\rangle_{-\varphi/2}-|\psi_1\rangle_{\varphi/2})/4 \quad (8)$$

with $\eta=0.2$ and $\eta Rt=0.8$, 1.2, 2.0, 3.0, and 6.0, respectively. According to Figs. 3 and 4, one may see that both $|\psi_1(t)\rangle_{\phi=0}$ and $|\psi_1(t)\rangle_{\phi=\pi}$ for the parameters selected here

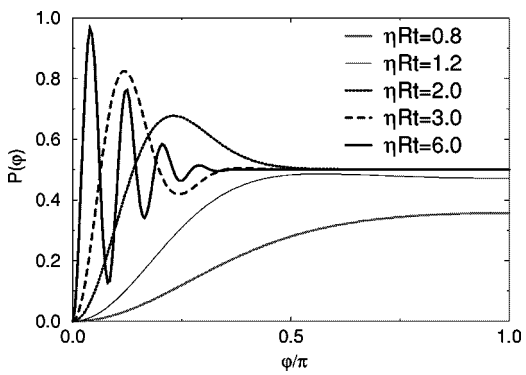

FIG. 14. The probability $P(\varphi)$ that the ion is in the $|g_2\rangle$ internal state and the $|S_-\rangle=(|\psi_1\rangle_{-\varphi/2}-|\psi_1\rangle_{\varphi/2})/2$ motional state. The LD parameter of the trapped ion is $\eta=0.2$.

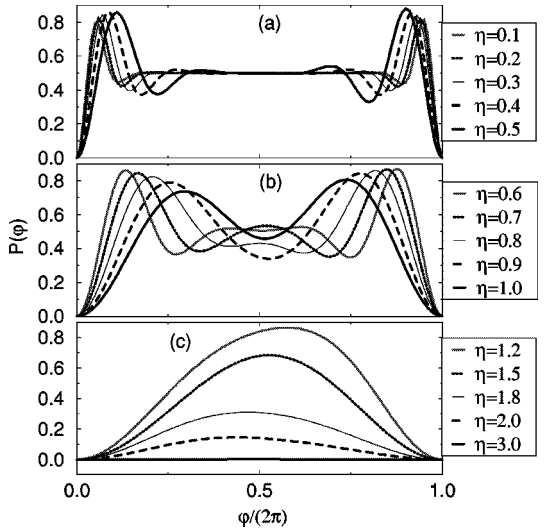

FIG. 15. The probability $P(\varphi)$ that the ion is in the $|g_2\rangle$ internal state and the $|S_-\rangle=(|\psi_1\rangle_{-\varphi/2}-|\psi_1\rangle_{\varphi/2})/2$ motional state. The parameters are selected as $\eta Rt=3.0$ and $\eta=0.1\sim0.5$ (a), $\eta=0.6\sim1.0$ (b), and $\eta=1.2$, 1.5, 1.8, 2.0, and 3.0 (c), respectively.

are of sub-Poissonian statistics and position-squeezing properties. However, the interference signals in Fig. 14 are similar to the experimental data and simple theoretical fits in Ref. [23]. This implies that theoretical calculations to the first order of the LD perturbation may give a quite good prediction for the interference signals, if the LD parameter and Raman excitation area are not too large. At first sight, it may seem strange that, though the quantum features of the displaced motional states $|\psi_1(t)\rangle_{\phi=0}$ deviate significantly from those of the coherent state, the interference signals differ less observably from those based on the first-order LD perturbation. Note that the quantum features of the displaced motional states $|\psi_1(t)\rangle_{\phi=\varphi/2}$ or $|\psi_1(t)\rangle_{\phi=-\varphi/2}$ depend strongly on $\varphi/2$, and that the squeezing properties and quantum statistics are related with the quantum fluctuation operators of $\tilde{z}$ or $\tilde{p}$ and Q value, respectively, while interference signals are related with the coherence between $|\psi_1(t)\rangle_{\phi=\varphi/2}$ and $|\psi_1(t)\rangle_{\phi=-\varphi/2}$. One may readily draw a conclusion that the quantum features of $|\psi_1(t)\rangle_{\phi=0}$ have little to do with the coherence between $|\psi_1(t)\rangle_{\phi=\varphi/2}$ and $|\psi_1(t)\rangle_{\phi=-\varphi/2}$. In Fig. 15, the interference signals are checked with $\eta Rt=3.0$ and various LD parameters $\eta=0.1$–3.0. It is shown that quantum interference can be observed over a wide range of localization conditions in spite of the complicated motional displacement caused by nonlinear vibrational couplings. We keep ηRt constant in our calculations because Raman displacements, to the first-order LD perturbation, are proportional to ηRt instead of Rt. This makes it easy to compare the effects from the nonlinear vibronic couplings under different localization conditions. One can see that, for small LD parameters, the interference signals are approximately symmetric over $\varphi=\pi$, i.e., $P(\pi+\varphi')\approx P(\pi-\varphi')$. But $P(\varphi)$ becomes nonsymmetric over $\varphi=\pi$ for large LD parameters.

It is clear that one has

$$P(\varphi)=P(-\varphi), \quad (9)$$

$$P(\varphi)=P(\varphi+4\pi), \tag{10}$$

which is valid under general Raman coupling and localization conditions. Note that

$$\mathcal{U}_{1,-\varphi}-\mathcal{U}_{1,\varphi}=\mathcal{U}^{\dagger}_{1,\varphi-\pi}-\mathcal{U}^{\dagger}_{1,\pi-\varphi}, \tag{11}$$

$$\mathcal{U}_{1,-\varphi}-\mathcal{U}_{1,\varphi}=\mathcal{U}^{\dagger}_{1,-\varphi-\pi}-\mathcal{U}^{\dagger}_{1,\pi+\varphi}. \tag{12}$$

We derive a symmetric relationship in the weak Raman coupling limit ($R\ll\nu$),

$$P(\varphi)=P(\varphi\pm 2\pi). \tag{13}$$

From Eqs. (9) and (13), we can immediately get

$$P(\pi+\varphi)=P(\pi-\varphi). \tag{14}$$

This symmetry exists for general localization conditions. But it become invalid when the nonresonant sideband transitions are taken into account. The effects from the nonresonant sideband transitions will be discussed elsewhere [36]. One can also see that the interference signals decrease with increasing η and finally approach zero for $\eta=3.0$. This indicates that $|\psi_1(t)\rangle_{-\varphi/2}$ and $|\psi_1(t)\rangle_{\varphi/2}$ spatially overlap, and that destructive interference occurs for the motional states $[|\psi_1(t)\rangle_{-\varphi/2}-|\psi_1(t)\rangle_{\varphi/2}]/2$. Though the Raman displacements are proportional to ηRt to the first-order LD perturbation, nonlinear modification becomes significant if the LD parameter is large. According to the above discussion concerning the first sideband Raman displacement, one may see that the displaced motional wave packets (from the motional ground state) in general spatially show a distribution with a wide oscillatory spread for weakly trapped ions. This implies that $|\psi_1(t)\rangle_{-\varphi/2}$ and $|\psi_1(t)\rangle_{\varphi/2}$ are not well-separated for any phase φ. The destructive interference between $|\psi_1(t)\rangle_{-\varphi/2}$ and $|\psi_1(t)\rangle_{\varphi/2}$ therefore causes the interference signal $P(\varphi)$ to decrease.

Briefly, we have studied quantum interferences of motional states of a trapped ion generated from the motional ground state by using the nonlinear coupling between electronic and vibrational degrees of freedom. Depending on the excitation parameters, the quantum statistics of these states were demonstrated to possess either sub-Poissonian or super-Poissonian character, while the position operator can show either squeezing or a distribution with a wide oscillatory spread. Quantum interferences were found to be less sensitive to the nonlinearity in the generation of the motional states and remain essentially unchanged up to very large LD parameters of the order of 1. The results obtained may be applied directly to the analysis of the experiment reported in Ref. [23], providing a more accurate description of the data (taken for $\eta=0.2$) than the linear coupling model.

V. CONCLUSION

In conclusion, we have discussed the Raman excitation and its application for the generation of nonclassical states of motion of a trapped ion under localization conditions in and beyond the LD limit. The nonlinear vibronic couplings in the Raman processes give rise to novel kinds of excitation of the vibrational ground state. The results were compared to the recent experiments in connection with the generation of coherent states, vacuum squeezed states, and ''Schrödinger cat'' states of the motion of the trapped $^{9}Be^{+}$ ion with the LD parameter $\eta\approx 0.2$ [18,23,37]. We note that a pure quantum-mechanical ground state of motion was recently attained with a probability of 98% [11] by the use of resolved-sideband stimulated Raman cooling. Further experiments with relatively large LD parameters can be achieved by adiabatically reducing the trap frequency. For example, one may double the LD parameter by decreasing the value of the trap frequency to its quarter. Because the trap frequency is changed adiabatically, the trapped ion will remain in the vibrational ground state with unchanged occupation probability [38]. On the other hand, if the well-defined quantum motional states can be generated in an ion trap under weak localization condition (i.e., with a relatively large LD parameter), the experimental observation of the nonlinearly modified Raman sideband excitations may become easy. As an interesting example, we consider a trapped $^{25}Mg^{+}$ ion in a miniature linear trap [39] with a trap frequency of $\nu=0.6$ MHz in the principal trap z axis. If the displacement Raman beams counterpropagate along the z axis with laser frequencies tuned to excite the atomic transitions $^{2}S_{1/2}\rightarrow{}^{2}P_{1/2}$, the LD parameter (for two-photon Raman transitions) may be as high as $\eta\approx 0.8$. In such a case, the motional superposition states obtained with displacement Raman beams are far away from Poissonian ones. Furthermore, one may experimentally decrease the LD parameter (for the z-dimensional motion) by either increasing the trap frequency or properly arranging the Raman beams to propagate along directions with certain angles with the principal trap z axis. Suppose that the applied laser beams propagate in directions of angles θ_1 and θ_2 with the z axis, respectively. We get a LD parameter $\eta=|\eta_1\cos(\theta_1)-\eta_2\cos(\theta_2)|$ with $\eta_i=\sqrt{\hbar k_i^2/2M\nu}(i=1,2)$. Therefore, it is possible to check the Raman excitations with various LD parameters. The results here are of particular interest with regard to the preparation of quantum and even nonclassical motional states and many-particle entangled states for two or more trapped ions in a linear trap [40–44].

ACKNOWLEDGMENTS

One of the authors (H.Z) acknowledges the financial support from the Japanese Science and Technology Agency (STA). Creative discussions with the ion-trap group of the Max-Planck Institute of Quantum Optics are gratefully acknowledged.

APPENDIX A

This appendix gives a derivation of the effective Hamiltonian for the Raman sideband transitions. We consider that a trapped ion interacts with the two applied laser fields by exciting electronic transitions between a hyperfine ground state $|1\rangle$ and intermediate states $|j\rangle$ with atomic transition frequency ω_j. The interaction can be described with the Hamiltonian

$$H=H_0+H_{tp}+H_{\rm int}, \tag{A1a}$$

$$H_0=\hbar\omega_j|j\rangle\langle j|, \tag{A1b}$$

$$H_{tp}=\hbar\nu\left(a^\dagger a+\frac{1}{2}\right), \tag{A1c}$$

$$H_{\rm int}=\hbar(g_1e^{ik_{1z}z-i\omega_{L1}t}+g_2e^{ik_{2z}z-i\omega_{L2}t})|j\rangle\langle 1|+\text{H.c.}, \tag{A1d}$$

where H_0 represents the internal energy, H_{tp} is the external energy of the trapped ion, $H_{\rm int}$ is the dipole couplings between the ground state $|1\rangle$ and intermediate state $|j\rangle$, g_1 and g_2 are, respectively, the associated single-photon coupling constants (complex), and $k_{1z}=\mathbf{e}_z\cdot\mathbf{k}_1$ and $k_{2z}=\mathbf{e}_z\cdot\mathbf{k}_2$ represent the components of the wave vectors of the applied laser beams in the z direction, respectively. The phases of the applied laser fields ($\phi_{1,2}$) are included in the complex coupling constants $g_{1,2}=|g_{1,2}|\exp(i\phi_{1,2})$.

It should be noted that the dipole couplings between the ground and intermediate states are accompanied by vibrational transitions which are determined by the position-dependent factors $\exp(\pm ik_{1z,2z}z)$. The dynamics of the system including internal and external degrees of freedom are governed by the master equation:

$$\frac{\partial}{\partial t}\rho=\frac{1}{i\hbar}[H,\rho]+\mathcal{L}_{\rm sp}\rho, \tag{A2}$$

where the Liouville operator $\mathcal{L}_{\rm sp}$ describes spontaneous emission

$$\mathcal{L}_{\rm sp}\rho=2\gamma_{j1}|1\rangle\tilde{\rho}_{jj}\langle 1|-2\gamma(|j\rangle\langle j|\rho+\rho|j\rangle\langle j|), \tag{A3}$$

where γ_{j1} is the spontaneous decay rate from the intermediate state $|j\rangle$ to the hyperfine ground state $|1\rangle$, and γ denotes the spontaneous decay rate out of the excited state $|j\rangle$. The latter normally includes spontaneous emission out of the related internal levels $|1\rangle$ and $|j\rangle$. Other ground-state sublevels are often experimentally depopulated by appropriate repumping laser beams. For simplicity, we neglect the mechanical effects due to spontaneous decay to (or repumping out of) sublevels other than $|1\rangle$. We use the symbol $\tilde{\rho}_{jj}$ to account for the spontaneous recoils, which are given by the integration over all the directions of the spontaneously emitted photons, weighted by an angular distribution function $W_\sigma(u)$,

$$\tilde{\rho}=\int_{-1}^{1}duW_\sigma(u)e^{-ik_0zu}\rho e^{ik_0zu}, \tag{A4}$$

where $k_0=\omega_j/c$. For a dipole transition, the angular distribution of the spontaneous emission takes the form $W_{\pm1}(u)=\frac{3}{8}(1+u^2)$ or $W_0=\frac{3}{4}(1-u^2)$ if the spontaneously emitted photon has a polarization $\sigma=\pm1$ or $\sigma=0$, respectively.

In order to study the effects of the quantized center-of-mass motion, we define the density matrix elements $\rho_{\xi,\zeta}(n,m)=\langle\xi,n|\rho|\zeta,m\rangle(\xi,\zeta=1,\text{ or }j)$, where $|n\rangle$ and $|m\rangle$ label the vibrational Fock states. Working in the interaction picture defined by the unitary transformation $\rho(t)=\mathcal{U}_0^\dagger(t)\rho\mathcal{U}_0(t)$ with $\mathcal{U}_0(t)=\exp[(1/i\hbar)H_0t]$, one can readily derive the equations of motion for the matrix elements from the master equation (A2), which read

$$\begin{aligned}\dot{\rho}_{1,1}(n,m)=&-i(n-m)\nu\rho_{1,1}(n,m)\\&-i\sum_{n_1}[g_1^*u^*_{n,n_1}(k_{1z})e^{-i\delta_1t}\\&+g_2^*u^*_{n,n_1}(k_{2z})e^{-i\delta_2t}]\rho_{j,1}(n_1,m)\\&+i\sum_{n_1}[g_1u_{n_1,m}(k_{1z})e^{i\delta_1t}\\&+g_2u_{n_1,m}(k_{2z})e^{i\delta_2t}]\rho_{1,j}(n,n_1)+2\gamma_{j1}\tilde{\rho}_{j,j}(n,m),\end{aligned} \tag{A5a}$$

$$\begin{aligned}\dot{\rho}_{j,1}(n,m)=&-i(n-m)\nu\rho_{j,1}(n,m)-i\sum_{n_1}[g_1u_{n,n_1}(k_{1z})e^{i\delta_1t}\\&+g_2u_{n,n_1}(k_{2z})e^{i\delta_2t}]\rho_{1,1}(n_1,m)\\&+i\sum_{n_1}[g_1u_{n_1,m}(k_{1z})e^{i\delta_1t}\\&+g_2u_{n_1,m}(k_{2z})e^{i\delta_2t}]\rho_{j,j}(n,n_1)-\gamma\rho_{j,1}(n,m),\end{aligned} \tag{A5b}$$

$$\begin{aligned}\dot{\rho}_{j,j}(n,m)=&-i(n-m)\nu\rho_{j,j}(n,m)-i\sum_{n_1}[g_1u_{n,n_1}(k_1)e^{i\delta_1t}\\&+g_2u_{n,n_1}(k_{2z})e^{i\delta_2t}]\rho_{1,j}(n_1,m)\\&+i\sum_{n_1}[g_1^*u^*_{n_1,m}(k_{1z})e^{-i\delta_1t}\\&+g_2^*u^*_{n_1,m}(k_{2z})e^{-i\delta_2t}]\rho_{j,1}(n,n_1)\\&-2\gamma\rho_{j,j}(n,m),\end{aligned} \tag{A5c}$$

where δ_1 and δ_2 represent the laser frequency detunings $\delta_1=\omega_j-\omega_{L1}$ and $\delta_2=\omega_j-\omega_{L2}$, respectively, and $u_{n_1,n_2}(k_z)$ is defined by $u_{n_1,n_2}(k_z)=\langle n_1|\exp(ik_zz)|n_2\rangle$.

If the applied laser fields are far off the atomic resonance, $|\delta_{1,2}|\gg\gamma,\gamma_{j1},\nu,|g_1|$, and $|g_2|$, the intermediate state can be adiabatically eliminated, and thus the interaction of the total system becomes

$$\frac{\partial}{\partial t}\rho=\frac{1}{i\hbar}[\hbar\nu a^\dagger a+H_{\rm eff},\rho]+\mathcal{L}_{\rm coh}\rho+\mathcal{L}_{\rm eff}\rho, \tag{A6a}$$

$$H_{\rm eff}=\hbar S|1\rangle\langle 1|+\hbar[Re^{i\Delta kz}e^{i(\delta_1-\delta_2)t}+\text{H.c.}]|1\rangle\langle 1|, \tag{A6b}$$

$$\begin{aligned}\mathcal{L}_{\rm coh}\rho=&-i\frac{\nu}{\delta^2}[\mathcal{C}^\dagger a^\dagger a\mathcal{C}\rho-\rho\mathcal{C}^\dagger a^\dagger a\mathcal{C}+a^\dagger a\rho\mathcal{C}^\dagger\mathcal{C}\\&-\mathcal{C}^\dagger\mathcal{C}\rho a^\dagger a],\end{aligned} \tag{A6c}$$

$$\mathcal{L}_{\rm eff}\rho=\mathcal{L}_1\rho+\mathcal{L}_2\rho, \tag{A6d}$$

$$\mathcal{L}_1\rho=\frac{2\gamma_{j1}}{\delta^2}\mathcal{C}\tilde{\rho}\mathcal{C}^\dagger-\frac{\gamma}{\delta^2}[\mathcal{C}^\dagger\mathcal{C}\rho+\rho\mathcal{C}^\dagger\mathcal{C}], \tag{A6e}$$

$$\mathcal{L}_2\rho=\frac{\gamma_{j1}\nu}{\delta^2\gamma}\int_{-1}^{1}duW_\sigma(u)e^{-ik_0zu}(\mathcal{A}\rho)e^{ik_0zu},$$

$$\mathcal{A}\rho=i[a^\dagger a\mathcal{C}\rho\mathcal{C}^\dagger+\mathcal{C}a^\dagger a\rho\mathcal{C}^\dagger-\text{H.c.}], \tag{A6f}$$

where the operator $\mathcal{C}$ is defined by $\mathcal{C}=g_1e^{ik_{1z}z+i\delta_1t}+g_2e^{ik_{2z}z+i\delta_2t}$, $\tilde{\rho}$ is defined as in Eq. (A4), and $\mathcal{L}_{\text{eff}}\rho$ and $\mathcal{L}_{\text{coh}}\rho$ represent the effective spontaneous damping and coherent couplings to the order of $1/\delta^2$, respectively, with $1/\delta\approx1/\delta_1\approx1/\delta_2$. H_{eff} represents the ac Stark shift of the internal ground state and the effective two-photon Raman interaction to the order of $1/|\delta|$. The ac Stark shift S is given by $S=(|g_1|^2+|g_2|^2)/\delta$, and the effective two-photon coupling constant R is defined by $R=g_1^*g_2/\delta$. In the above derivation, we used the assumption that the detunings $|\delta_1|$ and $|\delta_2|$ are much larger than $|\delta_1-\delta_2|,\nu,\gamma,|g_1|^2$, and $|g_2|^2$, and kept terms up to the order of $1/\delta^2$.

Note that all the terms in $\mathcal{L}_{\text{eff}}\rho$ and $\mathcal{L}_{\text{coh}}\rho$ scale as ν/δ^2 or γ/δ^2, while the two-photon Raman processes have an effective Rabi frequency and ac Stark shift proportional to $g_1^*g_2/\delta$ and $(|g_1|^2+|g_2|^2)/\delta$, respectively. In this paper, we consider the case of large laser frequency detunings where only the two-photon coupling indicated in H_{eff} is dominant. Moreover, the ac Stark shift is independent of the external motion. It produces no effects on Raman couplings between vibrational sidebands.

APPENDIX B

For large LD parameters η, the perturbation expansion of $\exp[i\Delta kz]$ in terms of η, as expressed in the Eq. (3), contains a lot of terms, which may become very difficult for numeric calculations. Additionally, if $\delta_1-\delta_2\neq l\nu_z(l=0,\pm1,\pm2,\ldots)$, the effective Hamiltonian expressed in Eq. (A6b) is time-dependent. If $R\sim\nu$, one should consider effects from the non-rotating-wave-approximation terms, since the vibrational rotating-wave approximation cannot be used. This appendix gives an efficient procedure to integrate the master equation governing the motion of a single trapped ion.

We rewrite the effective Hamiltonian for the interaction between Raman beams and a trapped ion as kinetic and potential operators,

$$H(t)=K+V(t), \tag{B1a}$$

$$K=\frac{p^2}{2m}, \tag{B1b}$$

$$V(t)=\frac{1}{2}m\nu^2z^2+2\hbar R\cos[i\Delta kz-i\Delta\omega t+i\phi]. \tag{B1c}$$

The time evolution of the system is given by

$$|\psi(t_i)\rangle=\mathcal{U}(t_i,t_{i-1})|\psi(t_{i-1})\rangle, \tag{B2}$$

where $|\psi(t_i)\rangle$ is the state of the system at $t=t_i(i=1,2,\ldots)$. In our cases, the trapped ion is assumed to be in the motional ground state $|0\rangle$ at $t=t_0$. $\mathcal{U}(t_i,t_{i-1})$ is the time-evolution operator, which satisfies the Schrödinger equation

$$\frac{d\mathcal{U}(t_i,t_{i-1})}{dt_i}=\frac{1}{i\hbar}H(t_i)\mathcal{U}(t_i,t_{i-1}). \tag{B3}$$

To integrate this equation, one may propagate the solution by a number of repeated short time propagations which can be performed accurately by using a splitting approximation and the fast Fourier transform (FFT) algorithm [45]. For a sufficiently short time interval $\Delta t=t_i-t_{i-1}$ during which $H(t)$ can be considered as a constant, the propagating operator $\mathcal{U}(t_i,t_{i-1})$ can be approximated by

$$\begin{aligned}\mathcal{U}(t_i,t_{i-1})&\approx\exp\left[-\frac{i}{\hbar}\Delta tH\left(\frac{t_i+t_{i-1}}{2}\right)\right]\\&=\exp\left\{-\frac{i\Delta t}{\hbar}\left[K+V\left(\frac{t_i+t_{i-1}}{2}\right)\right]\right\}\\&\approx\exp\left[-\frac{i\Delta t}{2\hbar}V\left(\frac{t_i+t_{i-1}}{2}\right)\right]\exp\left(-\frac{i\Delta t}{\hbar}K\right)\\&\quad\times\exp\left[-\frac{i\Delta t}{2\hbar}V\left(\frac{t_i+t_{i-1}}{2}\right)\right].\end{aligned} \tag{B4}$$

It can be readily shown that this approximation is accurate to the order $O(\Delta t)^2$. In order to use this approximation to propagate the solution, one starts with the state $|\psi(t_{i-1})\rangle$ at time $t=t_{i-1}$ in the position representations where the operator $\exp\{-i\Delta tV[(t_i+t_{i-1})/2]/(2\hbar)\}$ is a multiplicative factor, then by FFT switches to the momentum representation, where the operator $\exp[(-i\Delta t/\hbar)K]$ is a multiplicative factor. Finally, switching back to the position representation by an inverse Fourier transform and multiplying by the number $\exp\{-i\Delta tV[(t_i+t_{i-1})/2]/(2\hbar)\}$, one obtains the state $|\psi(t_i)\rangle$ at $t=t_i$.

Using the above procedure for numerical solution, one can easily calculate the Raman vibrational excitation of a trapped ion in the cases of weak confinement (large η), general detunings ($\Delta\omega\neq l\nu$), and strong Raman couplings (large R).

[1] For a recent review, see, for example, *Laser Manipulation of Atoms and Ions, Proceedings of the International School of Physics ''Enrico Fermi,'' Varenna, 1991*, edited by E. Arimondo and W. D. Phillips (North-Holland, Amsterdam, 1992).

[2] F. Diedrich and H. Walther, Phys. Rev. Lett. **58**, 203 (1987).

[3] W. Nagourney, N. Yu, and H. Dehmelt, Opt. Commun. **79**, 176 (1990); M. Schubert, I. Siemers, R. Blatt, W. Neuhauser, and P. E. Toschek, Phys. Rev. Lett. **68**, 3016 (1992).

[4] W. Nagourney, J. Sandberg, and H. G. Dehmelt, Phys. Rev. Lett. **56**, 2797 (1986); Th. Sauter, W. Neuhauser, R. Blatt, and

P. E. Toschek, *ibid.* **57**, 1696 (1986); J. C. Bergquist, R. G. Hulet, W. M. Itano, and D. J. Wineland, *ibid.* **57**, 1699 (1987); E. Peik, G. Hollemann, and H. Walther, Phys. Rev. A **49**, 402 (1994).

[5] R. Blatt, *Spectroscopy and Quantum Optics with Stored Ions*, in *Proceedings of the 14th International Conference on Atomic Physics*, edited by S. Smith, C. Wieman, and D. Wineland (AIP Press, New York, 1994), and references therein.

[6] C. A. Blockley, D. F. Walls, and H. Risken, Europhys. Lett. **14**, 761 (1991).

[7] C. A. Blockley and D. F. Walls, Phys. Rev. A **47**, 2115 (1993); J. I. Cirac, R. Blatt, A. S. Parkins, and P. Zoller, *ibid.* **49**, 1202 (1994).

[8] For the theory on the nonlinear JCM, see, for example, W. Vogel and D.-G. Welsch, Phys. Rev. A **40**, 7113 (1989), and references therein.

[9] W. Vogel and R. L. de Matos Filho, Phys. Rev. A **52**, 4214 (1995).

[10] F. Diedrich, J. C. Bergquist, W. M. Itano, and D. J. Wineland, Phys. Rev. Lett. **62**, 403 (1992).

[11] C. Monroe, D. M. Meekhof, B. E. King, S. R. Jefferts, W. M. Itano, D. J. Wineland, and P. Gould, Phys. Rev. Lett. **75**, 4011 (1995).

[12] S. E. Hamann, D. L. Haycock, G. Klose, P. H. Pax, I. H. Deutsch, and P. S. Jessen, Phys. Rev. Lett. **80**, 4149 (1998).

[13] J. I. Cirac, R. Blatt, A. S. Parkins, and P. Zoller, Phys. Rev. Lett. **70**, 762 (1993).

[14] J. Eschner, B. Appasamy, and P. E. Toschek, Phys. Rev. Lett. **74**, 2435 (1995).

[15] S. Wallentowitz, W. Vogel, I. Siemers, and P. E. Toschek, Phys. Rev. A **54**, 943 (1996).

[16] R. L. de Matos Filho and W. Vogel, Phys. Rev. Lett. **76**, 4520 (1996).

[17] J. I. Cirac, R. Blatt, and P. Zoller, Phys. Rev. A **49**, R3174 (1994).

[18] D. M. Meekhof, C. Monroe, B. E. King, W. M. Itano, and D. J. Wineland, Phys. Rev. Lett. **76**, 1796 (1996).

[19] R. Blatt, J. I. Cirac, and P. Zoller, Phys. Rev. A **52**, 518 (1995).

[20] D. J. Heinzen and D. J. Wineland, Phys. Rev. A **42**, 2977 (1990).

[21] J. Y. Poyatos, R. Walser, J. I. Cirac, P. Zoller, and R. Blatt, Phys. Rev. A **53**, R1966 (1996).

[22] J. I. Cirac, A. S. Parkins, R. Blatt, and P. Zoller, Phys. Rev. Lett. **70**, 556 (1993); H. Zeng and F. Lin, Phys. Rev. A **52**, 809 (1995); S. Gou, J. Steinbach, and P. Knight, *ibid.* **54**, R1014 (1996).

[23] C. Monroe, D. M. Meekhof, B. E. King, and D. J. Wineland, Science **272**, 1131 (1996), and references therein.

[24] R. L. de Matos Filho and W. Vogel, Phys. Rev. Lett. **76**, 608 (1996).

[25] J. F. Poyatos, J. I. Cirac, R. Blatt, and P. Zoller, Phys. Rev. A **54**, 1532 (1996).

[26] D. J. Wineland, J. J. Bollinger, W. M. Itano, and D. J. Heinzen, Phys. Rev. A **50**, 67 (1994); H. Zeng and F. Lin, *ibid.* **48**, 2393 (1993); **50**, R3589 (1994).

[27] S. Wallentowitz and W. Vogel, Phys. Rev. A **58**, 679 (1998); **55**, 4438 (1997).

[28] J. Steinbach, J. Twamley, and P. L. Knight, Phys. Rev. A **56**, 4815 (1997).

[29] S.-C. Gou and P. L. Knight, Phys. Rev. A **54**, 1682 (1996).

[30] H. Zeng, Phys. Rev. A **57**, 388 (1998).

[31] L. Mandel and E. Wolf, *Optical Coherence and Quantum Optics* (Cambridge University Press, New York, 1995); M. Hillery, Phys. Rev. A **36**, 3796 (1987); Opt. Commun. **62**, 135 (1987).

[32] I. L. Chuang, R. Laflamme, P. W. Shor, and W. H. Zurek, Science **270**, 1633 (1995); D. P. Divincenzo, *ibid.* **270**, 255 (1995); J. Cirac and P. Zoller, Phys. Rev. Lett. **75**, 3788 (1995); C. Monroe, D. M. Meekhof, B. E. King, W. M. Itano, and D. J. Wineland, *ibid.* **75**, 4714 (1995).

[33] J. I. Cirac, T. Pellizzari, and P. Zoller, Science **273**, 1207 (1996); W. H. Zurek, Phys. Today **44** (10), 36 (1991); D. M. Greenberger, M. A. Horne, and A. Zeilinger, *ibid.* **46** (8), 22 (1993); C. H. Bennett, *ibid.* **48** (10), 24 (1995).

[34] E. Schrödinger, Naturwissenschaften **23**, 807 (1935); **23**, 823 (1935); **23**, 844 (1935).

[35] See, for example, *Atom Interferometer*, edited by Paul R. Berman (Academic Press, 1997), and references therein.

[36] H. Zeng *et al.* (unpublished).

[37] S. R. Jefferts, C. Monroe, E. W. Bell, and D. J. Wineland, Phys. Rev. A **51**, 3112 (1995).

[38] J. Chen *et al.*, Phys. Rev. Lett. **69**, 1344 (1992); A. Kastberg *et al.*, *ibid.* **74**, 1542 (1995).

[39] C. A. Schrama, E. Peik, W. W. Smith, and H. Wather, Opt. Commun. **101**, 32 (1993).

[40] H. Walther, in *Proceedings of the Workshop on Light Induced Kinetic Effects on Atoms, Ions and Molecules*, edited by L. Moi, S. Gozzini, C. Gabbanini, E. Arimondo, and F. Strumia (ETS Editrice, Pisa, 1991), pp. 261–276.

[41] I. Waki, S. Kassner, G. Birkl, and H. Walther, Phys. Rev. Lett. **68**, 2007 (1992).

[42] G. Birkl, S. Kassner, and H. Walther, Nature (London) **357**, 310 (1992).

[43] M. R. Raizen, J. M. Gilligan, J. C. Bergquist, W. G. Itano, and D. J. Wineland, Phys. Rev. A **45**, 6493 (1992).

[44] H. Walther, Adv. At., Mol., Opt. Phys. **32**, 379 (1994), and refernces therein.

[45] R. Heater and H. Metium, J. Chem. Phys. **86**, 5009 (1987), and references therein.